Saarakkala, Seppo; Hinkkanen, Marko; Zenger, Kai

Speed control of two-mass mechanical loads in electric drives

Published in:
IEEE Energy Conversion Congress and Exposition (ECCE 2012)

DOI:
10.1109/ECCE.2012.6342673

Published: 15/09/2012

Document Version
Peer-reviewed accepted author manuscript, also known as Final accepted manuscript or Post-print

Please cite the original version:
Saarakkala, S., Hinkkanen, M., & Zenger, K. (2012). Speed control of two-mass mechanical loads in electric drives. In *IEEE Energy Conversion Congress and Exposition (ECCE 2012)* (pp. 1246-1253). https://doi.org/10.1109/ECCE.2012.6342673

Speed Control of Two-Mass Mechanical Loads in Electric Drives

Seppo E. Saarakkala*, Marko Hinkkanen*, and Kai Zenger§
Aalto University School of Electrical Engineering, P.O. Box 13000, FI-00076 Aalto, Helsinki, Finland
*Department of Electrical Engineering
§Department of Automation and Systems Technology

***Abstract*—This paper deals with model-based two-degrees-of-freedom (2DOF) speed control of two-mass systems. An analytic gain selection of a proportinal integral (PI) type feedback controller is proposed. The gains are given as functions of system parameters and desired dominant closed-loop poles. An analytic design of a prefilter is given to complete the 2DOF structure, using the pole-zero distribution of the feedback loop. The prefilter design covers step, ramp, and parabolic reference tracking. The proposed 2DOF controller is evaluated by means of simulations and experiments. The experimental setup consists of two 4-kW servo motors coupled together with a toothed belt. It was found that the proposed controller gives good reference tracking for step and dynamic commands as well as robust and fast load-torque rejection.**

I. Introduction

In recent years, electric drives are increasingly selected for a torque source in modern motion control devices. Problems may be encountered in a motion control system due to mechanical resonances, which are typically caused by power transmission components, such as gearboxes, drive trains, couplings, and belts [1], [2]. In order to cope with the mechanical difficulties, two-mass (or multi-mass) system models should be used for designing the control laws.

Two-mass systems are commonly controlled by means of 2DOF control, where regulation and command tracking properties are separated from each other [3], [4], [5]. Analytical model-based pole-placement rules for PI-type speed controller were proposed in [6]. The two gains of the PI-type controller were used to select equal coefficients (dampings or natural frequencies) for both the lower frequency poles and the higher frequency poles. In [7], the same rules were used in a PI-type feedback controller design, but the step-command tracking was improved by introducing flatness-based feedforward control. A comprehensive comparison between PI-type, state-feedback, and predictive controllers is given in [8].

The above-mentioned papers are focused only on the step-command tracking and the load-disturbance rejection characteristics. However, especially in servo applications, systems are often driven using dynamic (ramp or parabolic) references [9]. Moreover, the robustness analysis is often omitted or the robustness is verified after the controller design. In [10], robust model-based position and speed controllers were designed for a belt-driven system considering also the dynamic-reference tracking. However, analytic design rules were not given.

In this paper, an analytic design method for a 2DOF speed controller of a two-mass system is proposed. The main contributions of this paper are:

1) The gains of the PI-type feedback controller are given as functions of the system parameters and the desired dominant closed-loop poles, which enables high natural frequency of the feedback loop. Moreover, the process parameter variations can be taken into account already in the design phase of the controller.
2) An analytic design of a prefilter is given to complete the 2DOF structure, using the pole-zero distribution of the feedback loop. The prefilter design is given also for dynamic-command tracking.

The contents of the paper are as follows. A mechanical model of the two-mass system is given in Section II. The analytic design rules of the 2DOF speed controller are derived in Section III and a design example is given in Section IV. The designed controller is evaluated by means of simulations and experiments in Section V. The conclusions are given in Section VI.

II. System Model

The dynamics of the two-mass mechanical system are given as

$$J_{\mathrm{M}}\frac{d\omega_{\mathrm{M}}}{dt} = T_{\mathrm{M}} - T_{\mathrm{S}} - b\omega_{\mathrm{M}} \tag{1}$$

$$J_{\mathrm{L}}\frac{d\omega_{\mathrm{L}}}{dt} = T_{\mathrm{S}} - T_{\mathrm{L}} \tag{2}$$

$$T_{\mathrm{S}} = K_{\mathrm{S}}(\theta_{\mathrm{M}} - \theta_{\mathrm{L}}) + c_{\mathrm{S}}(\omega_{\mathrm{M}} - \omega_{\mathrm{L}}) \tag{3}$$

where the moments of inertia of the motor and the load are denoted by J_{M} and J_{L}, respectively. The angular speeds of the motor and the load are ω_{M} and ω_{L}, respectively. The viscous damping acting on the motor side is b. The motor electromagnetic torque, the loading torque, and the coupling torque are T_{M}, T_{L}, and T_{S}, respectively, and θ_{M} and θ_{L} are the angular positions of the motor and load, respectively. The angular speeds are the first time derivatives of the angular positions: $\omega_{\mathrm{M}} = d\theta_{\mathrm{M}}/dt$ and $\omega_{\mathrm{L}} = d\theta_{\mathrm{L}}/dt$. The torsional stiffness and the damping of the coupling are K_{S} and c_{S}, respectively.

If $b = 0$ is assumed, the open-loop transfer function from

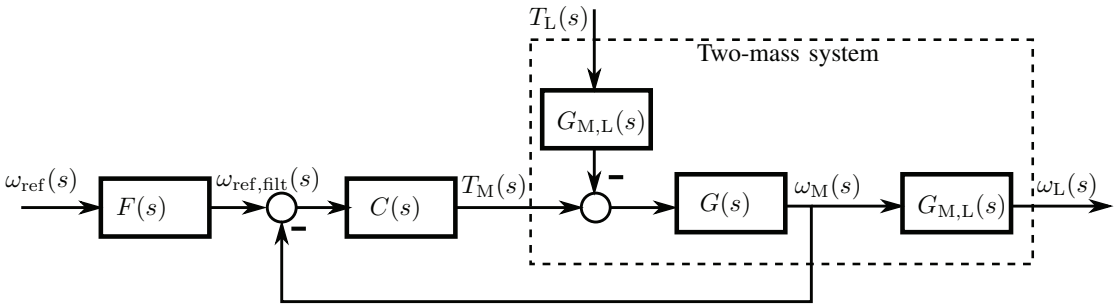

Fig. 1. 2DOF speed control structure. It is comprised of the feedback controller $C(s)$, the prefilter $F(s)$, and the two-mass system.

T_{M} to ω_{M} is obtained by Laplace transforming (1)…(3),

$$G(s) = \underbrace{\frac{1}{Js}}_{\text{Rigid part}} \underbrace{\frac{N_{\mathrm{M}}(s)}{D(s)}}_{\text{Flexible part}} \tag{4}$$

where $J = J_{\mathrm{M}} + J_{\mathrm{L}}$ and the numerator is given as

$$N_{\mathrm{M}}(s) = J_{\mathrm{L}}s^2 + c_{\mathrm{S}}s + K_{\mathrm{S}} \tag{5}$$

The denominator of the flexible part describes the resonant poles of the system

$$D(s) = \frac{J_{\mathrm{M}}J_{\mathrm{L}}}{J}s^2 + c_{\mathrm{S}}s + K_{\mathrm{S}} \tag{6}$$

The open-loop transfer function from T_{M} to ω_{L} is

$$G_{\mathrm{L}}(s) = \frac{1}{Js}\frac{N_{\mathrm{L}}(s)}{D(s)} \tag{7}$$

where the numerator is

$$N_{\mathrm{L}}(s) = c_{\mathrm{S}}s + K_{\mathrm{S}} \tag{8}$$

The transfer function from the motor speed ω_{M} to the load speed ω_{L} is defined as

$$G_{\mathrm{M,L}}(s) = \frac{N_{\mathrm{L}}(s)}{N_{\mathrm{M}}(s)} \tag{9}$$

If $c_{\mathrm{S}} = 0$ is assumed, the resonance and antiresonance frequencies are

$$\omega_{\mathrm{res}} = \sqrt{K_{\mathrm{S}}\frac{J}{J_{\mathrm{M}}J_{\mathrm{L}}}} \tag{10}$$

$$\omega_{\mathrm{ares}} = \sqrt{\frac{K_{\mathrm{S}}}{J_{\mathrm{L}}}} \tag{11}$$

respectively.

III. Speed Controller Design

In this section, an analytic design method of 2DOF speed control for two-mass systems is proposed. The speed control loop is illustrated in Fig. 1. It consists of the PI-type feedback controller $C(s)$ and the prefilter $F(s)$.

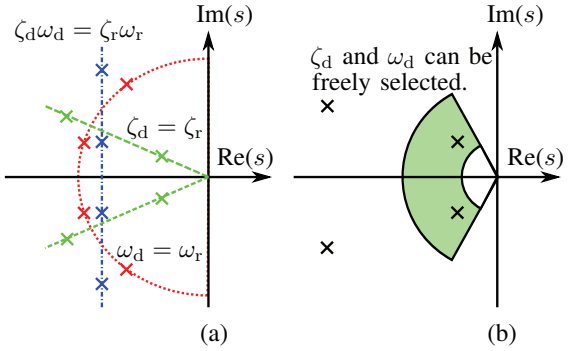

Fig. 2. Pole assignment techniques: (a) Identical damping coefficients (marked as green); identical real part (marked as blue); identical radius (marked as red), (b) Arbitrary selection of dominant poles.

A. Feedback Controller Design

The feedback controller is of PI type:

$$C(s) = k_{\mathrm{p}} + \frac{k_{\mathrm{i}}}{s}, \tag{12}$$

where k_{p} is the proportional gain and k_{i} is the integral gain. When the feedback loop is closed, the command-tracking transfer function from $\omega_{\mathrm{ref,filt}}$ to ω_{L} is

$$G_{\mathrm{c}}(s) = \frac{(k_{\mathrm{p}}s + k_{\mathrm{i}})N_{\mathrm{L}}(s)}{Js^2D(s) + (k_{\mathrm{p}}s + k_{\mathrm{i}})N_{\mathrm{M}}(s)} \tag{13}$$

and the load transfer function from T_{L} to ω_{M} is

$$G_{\mathrm{c,l}}(s) = -\frac{sN_{\mathrm{M}}(s)}{Js^2D(s) + (k_{\mathrm{p}}s + k_{\mathrm{i}})N_{\mathrm{M}}(s)} \tag{14}$$

The following requirements are set for the feedback-loop pole locations. The four poles of (13) are divided into two pairs of complex poles (dominant poles and resonant poles). Moreover, the coupling is assumed to be undamped (i.e., $c_{\mathrm{S}} = 0$). Thus, $G_{\mathrm{c}}(s)$ can be presented as

$$G_{\mathrm{c}}(s) = \frac{A(s + \frac{k_{\mathrm{i}}}{k_{\mathrm{p}}})}{\underbrace{(s^2 + 2\zeta_{\mathrm{d}}\omega_{\mathrm{d}}s + \omega_{\mathrm{d}}^2)}_{\text{Dominant poles}}\underbrace{(s^2 + 2\zeta_{\mathrm{r}}\omega_{\mathrm{r}}s + \omega_{\mathrm{r}}^2)}_{\text{Resonant poles}}} \tag{15}$$

where $A = \omega_{\mathrm{d}}^2\omega_{\mathrm{r}}^2k_{\mathrm{p}}/k_{\mathrm{i}}$.

Because the PI-type feedback controller only has two tunable parameters, the four closed-loop poles cannot be placed arbitrarily. Fig. 2(a) shows three pole-assignment techniques proposed in [6]: 1) identical damping coefficients; 2)

$$G_{\rm tot}(s)=\frac{\alpha s^2+\beta s+\gamma}{s^4+2(\zeta_{\rm r}\omega_{\rm r}+\zeta_{\rm l}\omega_{\rm l})s^3+(\omega_{\rm r}^2+\omega_{\rm l}^2+4\zeta_{\rm r}\zeta_{\rm l}\omega_{\rm r}\omega_{\rm l})s^2+2(\zeta_{\rm r}\omega_{\rm r}\omega_{\rm l}^2+\zeta_{\rm l}\omega_{\rm l}\omega_{\rm r}^2)s+\omega_{\rm r}^2\omega_{\rm l}^2} \tag{24}$$

$$e(s)=\omega_{\rm ref}(s)\frac{s^4+2(\zeta_{\rm r}\omega_{\rm r}+\zeta_{\rm l}\omega_{\rm l})s^3+(\omega_{\rm r}^2+\omega_{\rm l}^2+4\zeta_{\rm r}\zeta_{\rm l}\omega_{\rm r}\omega_{\rm l}-\alpha)s^2+[2(\zeta_{\rm r}\omega_{\rm r}\omega_{\rm l}^2+\zeta_{\rm l}\omega_{\rm l}\omega_{\rm r}^2)-\beta]s+\omega_{\rm r}^2\omega_{\rm l}^2-\gamma}{s^4+2(\zeta_{\rm r}\omega_{\rm r}+\zeta_{\rm l}\omega_{\rm l})s^3+(\omega_{\rm r}^2+\omega_{\rm l}^2+4\zeta_{\rm r}\zeta_{\rm l}\omega_{\rm r}\omega_{\rm l})s^2+2(\zeta_{\rm r}\omega_{\rm r}\omega_{\rm l}^2+\zeta_{\rm l}\omega_{\rm l}\omega_{\rm r}^2)s+\omega_{\rm r}^2\omega_{\rm l}^2} \tag{25}$$

identical real part; and 3) identical radius. In all of these pole-assignment techniques, the parameters of the feedback controller are used to select some coefficients (natural frequencies or dampings) of both the dominant and resonant poles. However, it is preferred to place the dominant and resonant poles into separate regions in the s-plane. Hence, it is more convenient to place only the dominant poles and then check that the resonant poles have enough damping. In the following, the PI-type feedback controller is designed so that the dominant poles can be arbitrarily placed, as depicted in Fig. 2(b).

The poles of the closed-loop system can be solved from the denominator polynomial of (13):

$$H(s)=Js^2D(s)+(k_{\rm p}s+k_{\rm i})N_{\rm M}(s) \tag{16}$$

The PI controller gains as a function of the system parameters and the dominant polepair coefficients ($\omega_{\rm d}$ and $\zeta_{\rm d}$) can be found through the following steps:

1) Substitute $s=-\sigma+{\rm j}\delta$, where $\sigma=\zeta_{\rm d}\omega_{\rm d}$ and $\delta=\omega_{\rm d}\sqrt{1-\zeta_{\rm d}^2}$, into (16).
2) Separate the real and imaginary parts of the equation:

$$\begin{aligned}H(s)&=h_1(J_{\rm M},J_{\rm L},K_{\rm S},k_{\rm p},k_{\rm i},\omega_{\rm d},\zeta_{\rm d})\\&+jh_2(J_{\rm M},J_{\rm L},K_{\rm S},k_{\rm p},k_{\rm i},\omega_{\rm d},\zeta_{\rm d})=0\end{aligned} \tag{17}$$

3) Solving the controller gains from the equation pair

$$\begin{aligned}h_1(J_{\rm M},J_{\rm L},K_{\rm S},k_{\rm p},k_{\rm i},\omega_{\rm d},\zeta_{\rm d})=0\\h_2(J_{\rm M},J_{\rm L},K_{\rm S},k_{\rm p},k_{\rm i},\omega_{\rm d},\zeta_{\rm d})=0\end{aligned} \tag{18}$$

leads to

$$k_{\rm p}=\frac{2J_{\rm M}\zeta_{\rm d}\omega_{\rm d}\left[\frac{K_{\rm S}J}{\omega_{\rm d}^2J_{\rm M}J_{\rm L}}+\frac{J_{\rm L}\omega_{\rm d}^2}{K_{\rm S}}+2(2\zeta_{\rm d}^2-1)\right]}{\frac{K_{\rm S}}{\omega_{\rm d}^2J_{\rm L}}+\frac{J_{\rm L}\omega_{\rm d}^2}{K_{\rm S}}+2(2\zeta_{\rm d}^2-1)} \tag{19}$$

$$k_{\rm i}=\frac{J_{\rm M}\omega_{\rm d}^2\left(\frac{K_{\rm S}J}{\omega_{\rm d}^2J_{\rm M}J_{\rm L}}+\frac{J_{\rm L}\omega_{\rm d}^2}{K_{\rm S}}-\frac{J}{J_{\rm M}}+4\zeta_{\rm d}^2-1\right)}{\frac{K_{\rm S}}{\omega_{\rm d}^2J_{\rm L}}+\frac{J_{\rm L}\omega_{\rm d}^2}{K_{\rm S}}+2(2\zeta_{\rm d}^2-1)} \tag{20}$$

4) Solve the remaining resonant polepair coefficients $\omega_{\rm r}$ and $\zeta_{\rm r}$. Equaling the denominator of (15) and $H(s)$ leads to

$$\omega_{\rm r}=\sqrt{\frac{k_{\rm i}K_{\rm S}}{\omega_{\rm d}^2J_{\rm M}J_{\rm L}}} \tag{21}$$

$$\zeta_{\rm r}=\frac{k_{\rm p}}{2J_{\rm M}\omega_{\rm r}}-\frac{\zeta_{\rm d}\omega_{\rm d}}{\omega_{\rm r}} \tag{22}$$

In the following, step-by-step design rules for the PI controller parameters are given. These rules are based on the system parameters and the coefficients of the dominant closed-loop polepair:

1) Select a minimum damping $\zeta_{\rm d}$ and a minimum natural frequency $\omega_{\rm d}$ for the dominant polepair of the feedback loop, corresponding to the worst-case closed-loop dynamics.
2) Calculate the feedback controller gains using (19) and (20) with the worst-case system parameter combination (i.e. maximum load inertia $J_{\rm L,max}$ and minimum coupling stiffness $K_{\rm S,min}$).
3) Calculate the resonant polepair coefficients using (21) and (22), needed in the prefilter design.

B. Prefilter Design

The command tracking from the angular speed reference $\omega_{\rm ref}$ to the load angular speed $\omega_{\rm L}$ is set by the prefilter. If the prefilter from $\omega_{\rm ref}$ to $\omega_{\rm ref,filt}$ is selected as

$$F(s)=\frac{(\alpha s^2+\beta s+\gamma)(s^2+2\zeta_{\rm d}\omega_{\rm d}s+\omega_{\rm d}^2)}{A(s+\frac{k_{\rm i}}{k_{\rm p}})(s^2+2\zeta_{\rm l}\omega_{\rm l}s+\omega_{\rm l}^2)} \tag{23}$$

the zero and the dominant poles of (15) are cancelled. The dynamics of the command tracking are selected by the design parameters α, β, γ, $\zeta_{\rm l}$, and $\omega_{\rm l}$, which can be, in theory, any positive real numbers. The natural frequency of the command-tracking dynamics should be selected clearly below the resonance frequency, meaning that $\omega_{\rm l}<\omega_{\rm r}$. The overall transfer function from $\omega_{\rm ref}$ to $\omega_{\rm L}$ is obtained multiplying (15) and (23) and it is given in (24).

Let us study the tracking error of the proposed 2DOF system. The tracking error $e(s)$ of the closed-loop system (24) can be expressed as

$$\begin{aligned}e(s)&=\omega_{\rm ref}(s)-\omega_{\rm L}(s)\\&=\omega_{\rm ref}(s)[1-G_{\rm tot}(s)]\end{aligned}$$

and it is given in (25). The steady-state tracking error $e_{\rm ss}$ can be solved from (25) applying the final value theorem

$$e_{\rm ss}=\lim_{t\to\infty}e(t)=\lim_{s\to0}se(s) \tag{26}$$

The design parameters α, β, γ are selected based on the command to be tracked. In the following, three typical cases are given:

1) Step-command tracking: $\omega_{\rm ref}(t)=v_{\rm ref}$, which is $\omega_{\rm ref}(s)=v_{\rm ref}/s$ in the s-domain. The steady-state tracking error can be solved using (25) and (26):

$$e_{\rm ss}=\frac{v_{\rm ref}(\omega_{\rm r}^2\omega_{\rm l}^2-\gamma)}{\omega_{\rm r}^2\omega_{\rm l}^2} \tag{27}$$

Zero steady-state tracking error without overshoot for a step command is reached, if $\alpha=\beta=0$ and $\gamma=\omega_{\rm r}^2\omega_{\rm l}^2$.

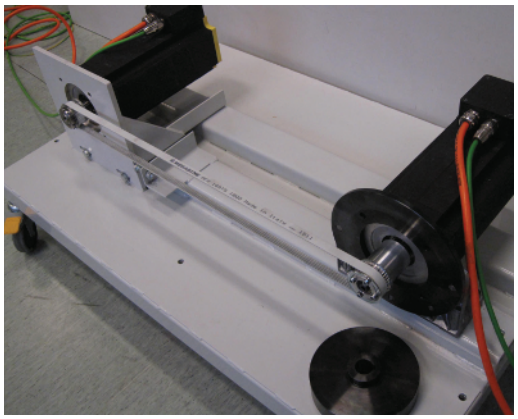

Fig. 3. Experimental two-mass system.

2) Ramp-command tracking: $\omega_{\mathrm{ref}}(t) = a_{\mathrm{ref}}t$, which is $\omega_{\mathrm{ref}}(s) = a_{\mathrm{ref}}/s^2$ in the s-domain. If $\gamma = \omega_{\mathrm{r}}^2\omega_{\mathrm{l}}^2$ is selected, the steady-state tracking error is

$$e_{\mathrm{ss}} = \frac{a_{\mathrm{ref}}[2(\zeta_{\mathrm{r}}\omega_{\mathrm{r}}\omega_{\mathrm{l}}^2 + \zeta_{\mathrm{l}}\omega_{\mathrm{l}}\omega_{\mathrm{r}}^2) - \beta]}{2(\zeta_{\mathrm{r}}\omega_{\mathrm{r}}\omega_{\mathrm{l}}^2 + \zeta_{\mathrm{l}}\omega_{\mathrm{l}}\omega_{\mathrm{r}}^2)} \tag{28}$$

Zero tracking error for a ramp command is reached, if $\alpha = 0$ and $\beta = 2(\zeta_{\mathrm{r}}\omega_{\mathrm{r}}\omega_{\mathrm{l}}^2 + \zeta_{\mathrm{l}}\omega_{\mathrm{l}}\omega_{\mathrm{r}}^2)$.

3) Parabolic-command tracking: $\omega_{\mathrm{ref}}(t) = j_{\mathrm{ref}}t^2$, which is $\omega_{\mathrm{ref}}(s) = j_{\mathrm{ref}}/s^3$ in the s-domain. If $\beta = 2(\zeta_{\mathrm{r}}\omega_{\mathrm{r}}\omega_{\mathrm{l}}^2 + \zeta_{\mathrm{l}}\omega_{\mathrm{l}}\omega_{\mathrm{r}}^2)$ and $\gamma = \omega_{\mathrm{r}}^2\omega_{\mathrm{l}}^2$ are selected, the steady-state tracking error is

$$e_{\mathrm{ss}} = \frac{j_{\mathrm{ref}}(\omega_{\mathrm{r}}^2 + \omega_{\mathrm{l}}^2 + 4\zeta_{\mathrm{r}}\zeta_{\mathrm{l}}\omega_{\mathrm{r}}\omega_{\mathrm{l}} - \alpha)}{\omega_{\mathrm{r}}^2 + \omega_{\mathrm{l}}^2 + 4\zeta_{\mathrm{r}}\zeta_{\mathrm{l}}\omega_{\mathrm{r}}\omega_{\mathrm{l}}} \tag{29}$$

Zero tracking error for parabolic command is reached, if $\alpha = \omega_{\mathrm{r}}^2 + \omega_{\mathrm{l}}^2 + 4\zeta_{\mathrm{r}}\zeta_{\mathrm{l}}\omega_{\mathrm{r}}\omega_{\mathrm{l}}$.

It is worth noticing that the prefilter transfer function (23) is not proper. The prefilter can, however, be implemented by dividing it into two parts:

$$\frac{\omega_{\mathrm{ref,filt}}(s)}{\omega_{\mathrm{ref}}(s)} = (\alpha s^2 + \beta s + \gamma)\underbrace{\frac{s^2 + 2\zeta_{\mathrm{d}}\omega_{\mathrm{d}}s + \omega_{\mathrm{d}}^2}{A(s + \frac{k_{\mathrm{i}}}{k_{\mathrm{p}}})(s^2 + 2\zeta_{\mathrm{l}}\omega_{\mathrm{l}}s + \omega_{\mathrm{l}}^2)}}_{F_{\mathrm{f}}(s)} \tag{30}$$

It can be seen that $\omega_{\mathrm{ref,filt}}(s)$ becomes

$$\begin{aligned}\omega_{\mathrm{ref,filt}}(s) &= [\alpha s^2\omega_{\mathrm{ref}}(s) + \beta s\omega_{\mathrm{ref}}(s) + \gamma\omega_{\mathrm{ref}}(s)]F_{\mathrm{f}}(s) \\ &= [\alpha j_{\mathrm{ref}}(s) + \beta a_{\mathrm{ref}}(s) + \gamma\omega_{\mathrm{ref}}(s)]F_{\mathrm{f}}(s)\end{aligned} \tag{31}$$

where $F_{\mathrm{f}}(s)$ is a proper transfer function. The prefilter can be implemented if the second time derivative j_{ref}, the first time derivative a_{ref}, and the speed reference ω_{ref} are available. Typically, the speed reference in motion control applications is generated from the second time derivative (i.e. the jerk signal) and then integrated two times to get first the acceleration reference and finally the speed reference. Methods for jerk-bounded trajectory planning has been proposed, e.g., in [11] and [12].

IV. Design Example

In this section, the analytic design rules are applied to speed control of tooth-belt driven two-mass system.

TABLE I
System Parameters

Parameter	Value
J_{M}	0.005 kgm^2
J_{L}	$[0.005, 0.038]$ kgm^2
b	0.01 Nms/rad
K_{S}	$[700, 1100]$ Nm/rad
c_{S}	$K_{\mathrm{s}}/4000$ Nms/rad
ω_{res}	$[398, 663]$ rad/s
ω_{ares}	$[136, 469]$ rad/s

A. Experimental Setup

The experimental setup considered in this section is shown in Fig. 3. The setup consists of two 4-kW 2400-rpm servo motors coupled together with a toothed belt. In order to vary the coupling stiffness, different belts can be used. An addional inertia disk can be added to the shaft of the load motor. The parameters and the estimated resonance frequencies of the system are given in Table I. Two different mechanical parameter sets are considered in this paper. The first parameter set ($J_{\mathrm{M}} = 0.005$ kgm^2, $J_{\mathrm{L}} = 0.005$ kgm^2, $K_{\mathrm{S}} = 1100$ Nm/rad) produces the antiresonance and resonance frequencies near to each other. On the other hand, the second parameter set ($J_{\mathrm{M}} = 0.005$ kgm^2, $J_{\mathrm{L}} = 0.038$ kgm^2, $K_{\mathrm{S}} = 700$ Nm/rad) produces the resonance frequencies far away from each other. The second parameter set is referred to a worst-case set in the following.

B. 2DOF Controller Design

When designing the 2DOF controller, it is required that the feedback loop is fast and it has to remain robustly stable in the system parameter range given in Table I. Similar parameter range can be found, e.g., from an industrial tooth-belt drive [13]. Moreover, the prefilter is used to improve the command tracking.

To guarantee fast closed-loop dynamics, the lower limit for the natural frequency of the dominant poles is set as $\omega_{\mathrm{d}} > \omega_{\mathrm{ares,min}}/4$, where $\omega_{\mathrm{ares,min}}$ is the minimum antiresonance frequency, which can be calulated from (11) using maximum load inertia and minimum coupling stiffness. To place the dominant and resonant poles into separate regions in the s-plane, another limit is set as $\omega_{\mathrm{d}} < \omega_{\mathrm{ares,min}}$. Moreover, to get robustly stable and sufficiently damped feedback-loop dynamics, the limit for the damping of the dominant poles is set as $0.2 < \zeta_{\mathrm{d}} < 1$. It is worth noticing that it may be useful to plot the PI controller parameters as functions of the dominant polepair coefficients when selecting the dominant closed-loop dynamics. Depending on the noise level of the feedback signal, the control designer may have variety of choices how to select the coefficients of the dominant polepair.

As an example, Fig. 4 shows the contours of the speed controller gains as functions of ω_{d} and ζ_{d}. The worst-case system parameter combination ($K_{\mathrm{S}} = 700$ Nm/rad, $J_{\mathrm{M}} = 0.005$ kgm^2, and $J_{\mathrm{L}} = 0.038$ kgm^2) is used. In practise, the proportional gain is limited by the measurement noise level. It can be seen in Fig. 4(a) that the coefficients of dominant poles can be freely selected from the contour indicating the given gain.

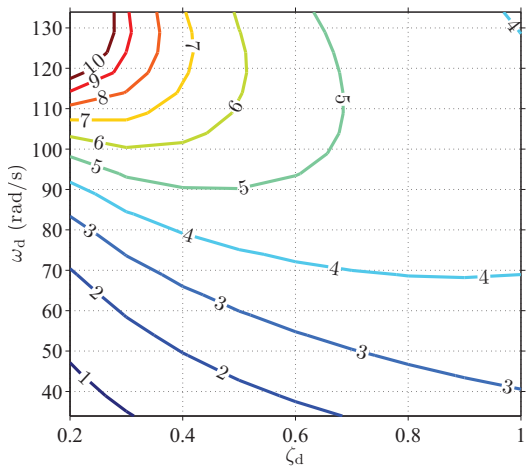

(a)

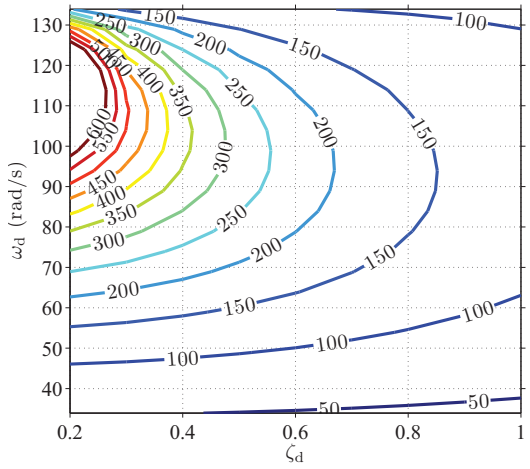

(b)

Fig. 4. PI controller gains when the coefficients of the dominant poles are varied ($0.2 < \zeta_\mathrm{d} < 1$ and $\omega_{\mathrm{ares,min}}/4 < \omega_\mathrm{d} < \omega_{\mathrm{ares,min}}$): (a) Proportional gain k_p (Nms/rad), (b) Integral gain k_i (Nm/rad).

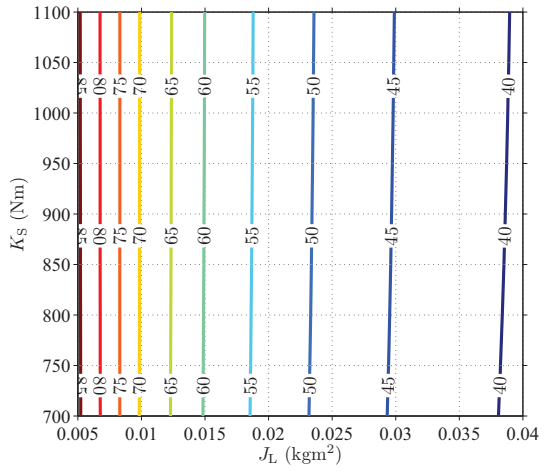

(a)

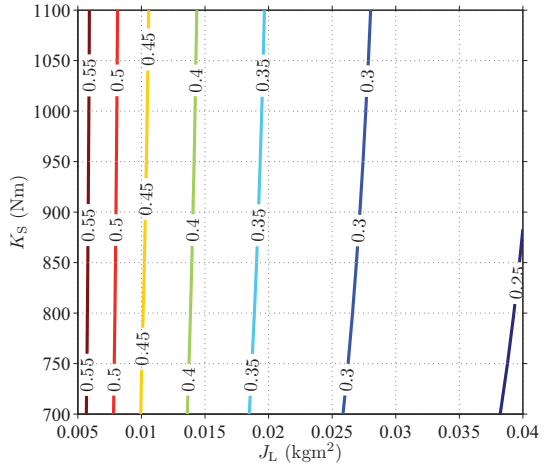

(b)

Fig. 5. Coefficients of the dominant poles when the system parameters are varied: (a) Natural frequency ω_d (rad/s), (b) Damping ζ_d.

In the experimental setup, the angular speed is calculated from the measured angular position difference within the fixed sampling interval of 1 ms. The described method causes quantification noise especially at low rotational speeds. For this reason, the feedback controller is designed for good noise sensitivity. Thus, according to Fig. 4(a), $\omega_\mathrm{d} = 40$ rad/s and $\zeta_\mathrm{d} = 0.25$ are selected. The prefilter is used to improve the command-tracking properties by introducing faster and better damped dominant dynamics: $\omega_\mathrm{l} = 100$ rad/s and $\zeta_\mathrm{l} = 1$.

C. Robustness

It is beneficial to analyze the robustness of the controller against the system parameter inaccuracies before the controller is implemented. In this section, both the robust stability and the robust performance are addressed.

Only the feedback controller $C(s)$ affects the robust stability. Hence, it is sufficient to analyze the poles of the closed-loop system (13) in parameter range given in Table I. The load inertia J_L and the coupling stifness K_S are the varying parameters. Fig. 5 shows the coefficients of the dominant poles as functions of J_L and K_S. The coefficients of the dominant poles are as designed, when the worst-case system parameter combination is used. When the parameters vary, both the damping and the natural frequency of the dominant poles are increased. Fig. 6 shows the coefficients of the resonant poles as functions of J_L and K_S. When comparing the natural frequencies of the dominant poles and the resonant poles in Figs. 5(a) and 6(a), it can be seen that the natural frequency of the resonant poles is clearly higher. Moreover, it can be seen in Fig. 6(b) that the damping of the resonant poles is sufficient ($\zeta_\mathrm{r} > 0.16$) in the whole parameter range. These observations mean that the dominant poles describe the dynamics of the feedback loop, and thus, it can be concluded that robustly stable feedback loop is obtained.

The second issue is to check the robust performance of the designed 2DOF control system. The parameter variation only affects the numerator of the prefilter (23), meaning that the

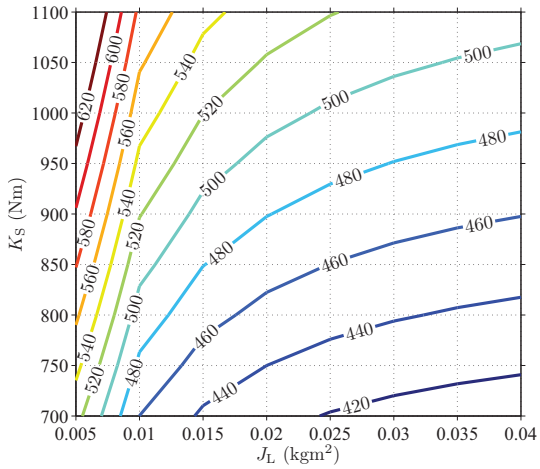

(a)

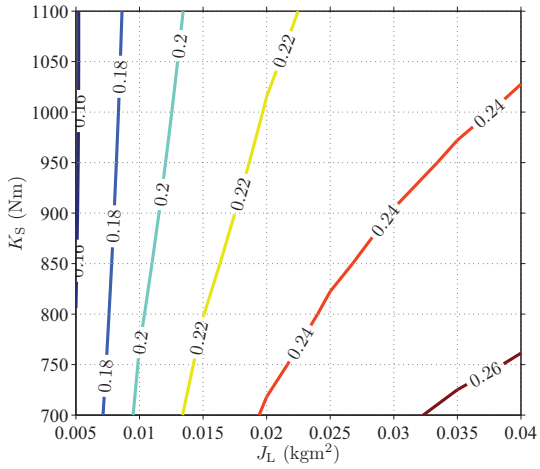

(b)

Fig. 6. Coefficients of the resonant poles when the system parameters are varied: (a) Natural frequency ω_r (rad/s), (b) Damping ζ_r.

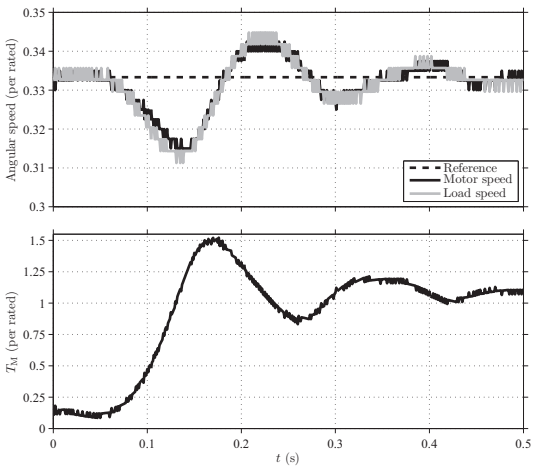

(a)

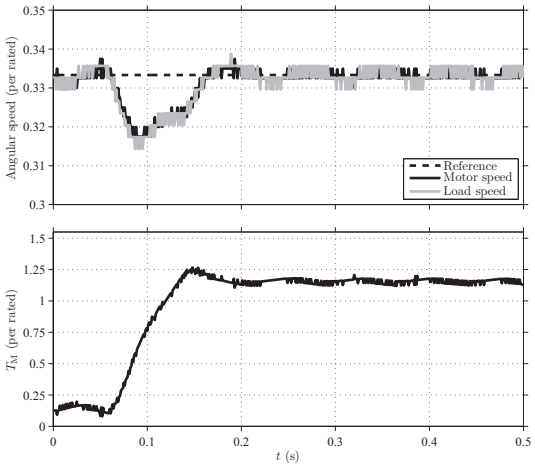

(b)

Fig. 7. Measured load-torque rejection of the PI-controlled two-mass system: (a) System parameters are correct, (b) Maximum parameter errors.

cancellation of the zero of (15) is valid even if the parameters of the system vary. On the other hand, the attempt to cancel the dominant poles will affect to the command tracking capability when the system parameters vary, because the coefficients of the dominant poles will change. However, it can be seen in Fig. 5 that the load inertia J_L mainly affects the change of the dominant-pole coefficients. The robust performance could be guaranteed by introducing a prefilter with coefficients as functions of load inertia J_L and coupling stifness K_S according to Figs. 5 and 6. In this paper, constant coefficients (calculated using the worst-case system parameter combination) are used in the prefilter and the command-tracking performance is evaluated in simulations and experiments using erroneous system parameter combinations.

V. Results

The designed 2DOF speed controller is evaluated by means of simulations and experiments. The tests are carried out using the two-mass system with the following parameter values: $K_S = 700$ Nm/rad, $c_S = K_S/4000$ Nms/rad, and $J_L = 0.038$ kgm^2. The design parameters are: $\omega_d = 40$ rad/s; $\zeta_d = 0.25$; $\omega_l = 100$ rad/s and $\zeta_l = 1$. These parameters lead to the resonant-pole coefficients $\omega_r = 410$ rad/s and $\zeta_r = 0.22$.

A. Load-Torque Rejection

Load-torque rejection of the feedback loop is tested at speed of 1/3 per rated. Fig. 7(a) shows the measured motor speed and the load speed, when the system parameters are correct ($K_S = 700$ Nm/rad, $c_S = K_S/4000$ Nms/rad, and $J_L = 0.038$ kgm^2). Fig. 7(b) shows the measured motor speed and the load speed with maximum parameter errors ($K_S = 1100$ Nm/rad, $c_S = K_S/4000$ Nms/rad, and $J_L = 0.005$ kgm^2). In both tests, a rated load-torque step is applied at $t = 0.05$ s. When the system parameters are correct, both the damping and the dominant natural frequency of the feedback loop are clearly lower than in the case with maximum parameter errors. This observation agrees with analysis in Section IV-C.

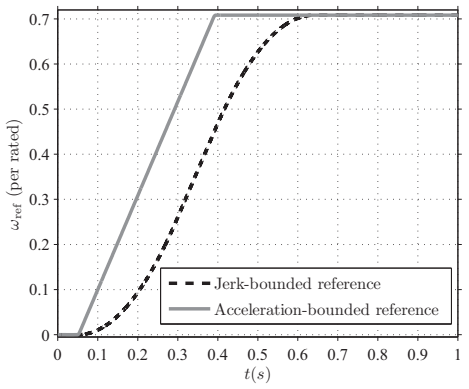

Fig. 8. Bounded speed references considered in the command tracking tests.

B. Command Tracking

Command tracking of the designed controllers is tested in simulations and experiments. Both the 1DOF, i.e. $F(s) = 1$, and 2DOF controllers are considered. Moreover, the controllers are compared to an acceleration feedforward structure, which is a well-known method in industrial applications [9]. In the acceleration feedforward, a feedforward torque $T_{\rm FF} = Ja_{\rm ref}$ is added to the output of the feedback controller $C(s)$. The responses are shown for three speed references: the step reference; the jerk-bounded reference (i.e. parabolic reference); and the acceleration-bounded reference (i.e. ramp reference). The shape of the bounded references are shown in Fig. 8. The step-response tests are performed using the experimental setup while the tracking of the bounded references is tested in simulations.

Fig. 9 shows the results of the step-response tests. It can be seen in Fig. 9(a) that when the system parameters are correct, the system behaves according to the analyses. The 1DOF PI controller gives a fast step response but there is an overshoot and oscillations because the damping of the feedback loop is low ($\zeta_{\rm d} = 0.25$). The proposed 2DOF PI controller gives better response; it is fast and there is no overshoot. Fig. 9(b) shows that an acceptable step response is obtained for the 2DOF PI controller with maximum parameter errors.

Fig. 10 shows the results of the parabolic-response tests when the system parameters are correct. It can be seen that the proposed 2DOF PI controller gives better tracking performance than the 1DOF control or the 1DOF control with the acceleration feedforward structure. The reason is that the prefilter is designed to ideally give zero steady-state tracking error also for parabolic commands.

Fig. 11 shows the results of the ramp-response tests. It can be seen in Fig. 11(a) that when the system parameters are correct, the proposed 2DOF PI controller reduces the ramp-command tracking error compared to the 1DOF structure (both with and without the acceleration feedforward). Fig. 11(b) shows the results with maximum parameter errors. It can be seen that the 1DOF controller gives smaller tracking error than the 2DOF controller and the 1DOF controller with the acceleration feedforward. It is worth noticing that the proposed 2DOF structure tolerates well the parameter error in coupling stiffness $K_{\rm S}$ as can be seen by comparing Figs. 11(a) and 11(c). It was found out that even with highly erroneous parameter values (57% in $K_{\rm S}$ and 50% in $J_{\rm L}$) the 2DOF PI controller still outperforms the 1DOF controller in ramp-reference tracking.

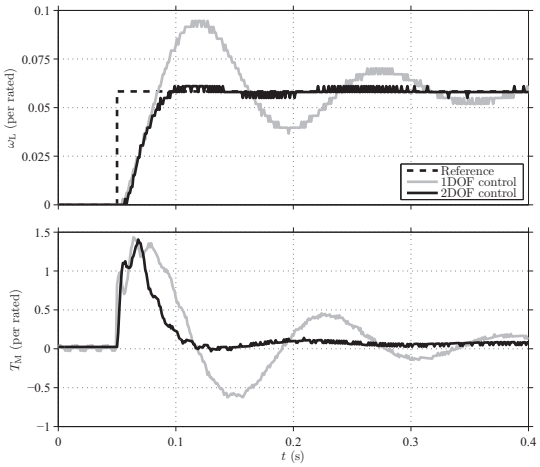

(a)

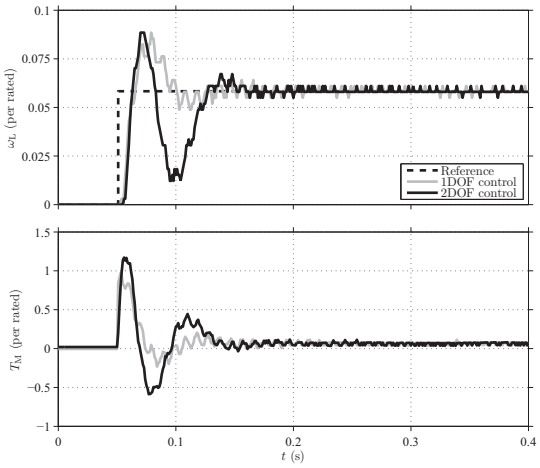

(b)

Fig. 9. Measured step responses: (a) Parameters are correct, (b) Maximum parameter errors (87% in $J_{\rm L}$ and 57% in $K_{\rm S}$).

VI. Conclusions

A systematic design method for 2DOF PI speed control of two-mass mechanical loads is proposed in this paper. The design rules for controller parameters are obtained using model-based pole-placement methods, taking into account the system parameter variations. It was shown by simulations and experiments that the designed controller gives good reference tracking for step and dynamic commands as well as robust and fast load-torque rejection.

Acknowledgment

The authors gratefully acknowledge ABB Oy for the financial support.

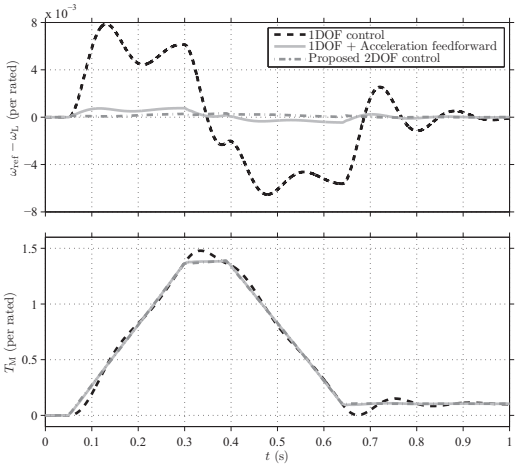

Fig. 10. Simulated tracking of parabolic reference.

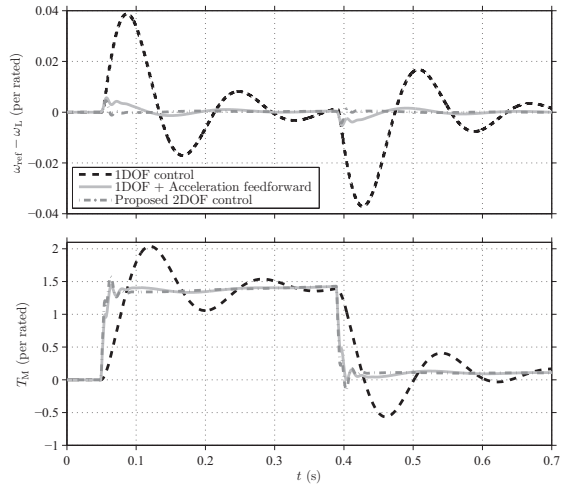

(a)

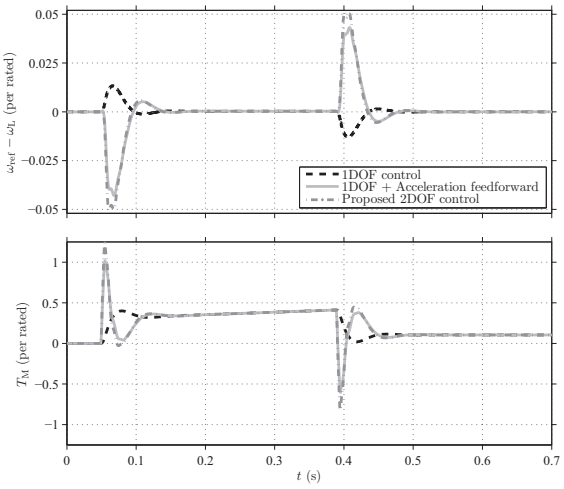

(b)

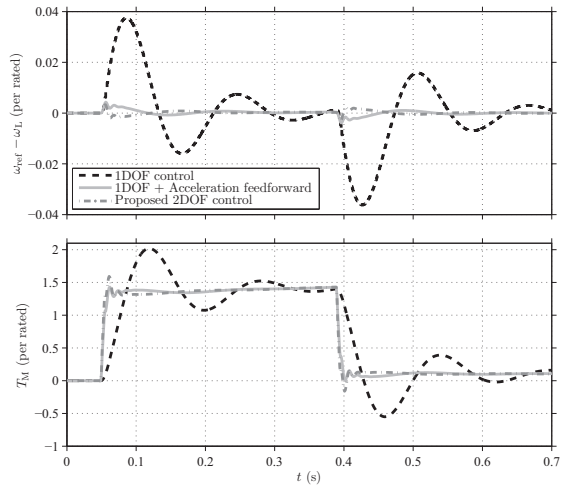

(c)

Fig. 11. Simulated tracking of ramp reference: (a) Parameters are correct, (b) Maximum parameter errors (87% in J_L and 57% in K_S), (c) Maximum parameter error (57%) in K_S.

REFERENCES

[1] M. Valenzuela, J. Bentley, and R. Lorenz, "Evaluation of torsional oscillations in paper machine sections," *IEEE Trans. Ind. Appl.*, vol. 41, no. 2, pp. 493–501, Mar.-Apr. 2005.

[2] M. Valenzuela, J. Bentley, P. Aguilera, and R. Lorenz, "Improved coordinated response and disturbance rejection in the critical sections of paper machines," *IEEE Trans. Ind. Appl.*, vol. 43, no. 3, pp. 857–869, May-Jun. 2007.

[3] R. Dhaouadi, K. Kubo, and M. Tobise, "Two-degree-of-freedom robust speed controller for high-performance rolling mill drives," *IEEE Trans. Ind. Appl.*, vol. 29, no. 5, pp. 919–923, Sep./Oct. 1993.

[4] K. Saiki, A. Hara, K. Sakata, and H. Fujimoto, "A study on high-speed and high-precision tracking control of large-scale stage using perfect tracking control method based on multirate feedforward control," *IEEE Trans. Ind. Electron.*, vol. 57, no. 4, pp. 1393–1400, Apr. 2010.

[5] M. Iwasaki, K. Seki, and Y. Maeda, "High-precision motion control techniques: A promising approach to improving motion performance," *IEEE Ind. Electron. Mag.*, vol. 6, no. 1, pp. 32–40, Mar. 2012.

[6] G. Zhang and J. Furusho, "Speed control of two-inertia system by PI/PID control," *IEEE Trans. Ind. Electron.*, vol. 47, no. 3, pp. 603–609, Jun. 2000.

[7] S. Thomsen and F. W. Fuchs, "Design and analysis of a flatness-based control approach for speed control of drive systems with elastic couplings and uncertain loads," in *EPE European Conference on Power Electronics and Applications*, Birmingham, UK, Aug. 2011, CD-ROM.

[8] S. Thomsen, N. Hoffmann, and F. W. Fuchs, "PI control, PI-based state space control, and model-based predictive control for drive systems with elastically coupled loads — a comparative study," *IEEE Trans. Ind. Electron.*, vol. 58, no. 8, pp. 3647–3657, Aug. 2011.

[9] G. Ellis, *Control System Design Guide: A Practical Guide*. San Diego, California: Elsevier, 2004.

[10] M. Jokinen, *Centralized motion control of a linear tooth belt drive: analysis of the performance and limitations*, D.Sc. Dissertation, Lappeenranta University of Technology, Lappeenranta, Finland, 2010.

[11] S. Macfarlane and E. Croft, "Jerk-bounded manipulator trajectory planning: design for real-time applications," *IEEE Trans. Robot. Autom.*, vol. 19, no. 1, pp. 42–52, Feb. 2003.

[12] H. Li, M. Le, Z. Gong, and W. Lin, "Motion profile design to reduce residual vibration of high-speed positioning stages," *IEEE/ASME Trans. Mechatronics*, vol. 14, no. 2, pp. 264–269, Apr. 2009.

[13] M. Jokinen, S. Saarakkala, M. Niemela, R. Pollanen, and J. Pyrhonen, "Physical drawbacks of linear high-speed tooth belt drives," in *International Symposium on Power Electronics, Electrical Drives, Automation and Motion (SPEEDAM)*, Jun. 2008, pp. 872–877.